Kinematic Analysis of a Two Degree-of-freedom Parallel Manipulator

Liang Yan, I-Ming Chen, Chee Kian Lim
School of Mechanical and Aerospace Engineering
Nanyang Technological University, Singapore 639798
yanliang@pmail.ntu.edu.sg, michen@ntu.edu.sg

***Abstract*—This paper presents a new design of two degree-of-freedom (2-DOF) non-symmetric parallel mechanism which can be employed as humanoid arm structure. Unlike conventional multi-DOF parallel mechanism, this design targets to reduce the number of actuators, and thus the total cost. The major feature of this mechanism is that it can move an end-effector in six-dimension (6D) space with only two motors, including three translational and three rotational motions. The forward, inverse kinematics as well as workspace of this parallel manipulator is analyzed and visualized. A prototype is developed and successfully implemented into the robotic lion dancing system as a humanoid arm structure.**

***Index Terms*—arm structure, parallel mechanism**

I. Introduction

A parallel manipulator is a closed-loop kinematic chain mechanism whose end-effector is linked to the base by several independent kinematic chains. So far, the most commonly studied parallel mechanism is the six degree-of-freedom (6-DOF) manipulator proposed by Gough $et\ al$ [1], which is currently well-known as Stewart Platform. The name of Stewart was attached to this architecture because Gough's earlier work (and a photograph of his platform) were mentioned in the reviewers' remarks to a paper by Stewart [2] published in 1965. A Stewart platform can achieve 6-DOF motions (x, y, z, pitch, roll, yaw) with three legs having two motors each. Merlet [3] presented a method for designing optimal parallel manipulators of the Gough platform type, according to design constraints like a specified workspace, best accuracy over the workspace, minimum articular forces for a given load, etc. In some circumstances, it is not necessary to generate 6-DOF motions of the end-effector. Therefore, less-DOF mechanism designs are proposed by researchers to reduce the number of actuators, and thus the total cost. Li $et\ al.$ [4] performed the type synthesis of 5-DOF parallel manipulators systematically by the constraint-synthesis method. Kong $et\ al.$ [5] proposed a general method for the type synthesis of 5-DOF parallel manipulators based on screw theory and using the concept of virtual chains. A novel parallel manipulator architecture was introduced by Angeles $et\ al.$ [6] to produce 4-DOF SCARA (Selective-Compliance Assembly Robot Arm) motions. Richard $et\ al.$ [7], [8] presented a 4-DOF parallel manipulator which can generate translations in all directions and rotation around an axis of a fixed direction. In the machine tool industry, manufacturers have introduced several 3-DOF parallel machines over the last decade. Most of these machines are based on the Delta robot [9], a translational 3-DOF parallel mechanism. The design of a spherical 3-DOF parallel manipulator was considered by Gosselin $et\ al.$ [10] from a kinematic viewpoint using criteria of symmetry, workspace maximization, and isotropy. Lee $et\ al.$ [11] presented a 3-DOF manipulator that can achieve two rotational motions and one translational motion based on the concept of in-parallel actuated mechanism. Another 3-DOF spatial parallel manipulator is proposed by Carretero $et\ al.$ [12], [13] to achieve the tipping, tilting and focusing of the secondary mirror of a telescope.

Most parallel mechanisms proposed by previous researchers use symmetric architecture, i.e., the legs and corresponding joints in those parallel mechanisms are the same. This type of mechanism has its advantages such as easiness for control implementation, convenience for assembling etc. However, for certain particular motions of end-effector, the symmetric architecture may take more actuators and special joints (spherical or universal) to achieve the motion, which increases the system cost. Therefore, in this paper, an asymmetric architecture is utilized to build up a parallel mechanism to achieve the end-effector motion by using reduced number of actuators. Specifically, two motors are employed to design a humanoid arm structure, and to achieve the motion of an end-effector in six directions, four of which are parasitic motions. Unlike conventional design, this parallel humanoid arm structure does not target to reduce the parasitic motions, because the parasitic motions are also useful in some cases such as the humanoid in a lion dancing system that can perform life-size lion dancing with the traditional lion dance outfit to generate a lively effect of the lion head.

The subsequent sections are organized as follows. In Section II, the architecture of the 2-DOF parallel manipulator is described. Following that, the system kinematic is analyzed in Section III. Subsequently, the inverse kinematics analysis of this arm structure is presented in Section IV. After that, the workspace of this mechanism is computed and visualized in Section V. In the end, the paper is concluded in Section VII.

II. Concept Design

A. Description of the Arm Structure

Figure 1 presents the proposed design of the humanoid arm structure. Generally speaking, compared with the serial mechanisms used in normal robot arms, parallel mechanisms have the following merits [12].

978–1–4244–1676–9/08/$25.00

- High payload capacity;
- High stiffness realized due to its truss structure;
- High-speed and acceleration, because of the non-accumulation of link's weight in one of the actuators;
- High static and dynamic accuracy, because of non-accumulation axial positioning errors.

Therefore, in this study, parallel mechanism is employed for the concept design of the humanoid arm structure.

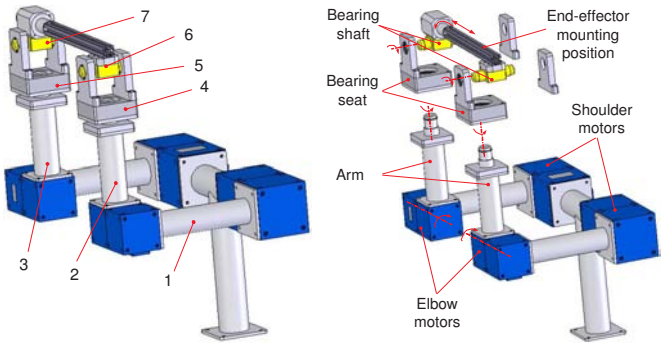

(a) Assembly view (b) Exploded view

Fig. 1. Concept design of humanoid arm structure of robotic lion

Joints and motions in the humanoid arm structure are illustrated in Fig. 1(b). Two motors are used as the shoulders, and the other two are employed as the elbows. Two bearing seats mounted on top of the two arms can rotate about the arms' axes. Two bearing shafts are used to support the bar on the top of the mechanism, where the end-effector such as lion head can be mounted. One side of the bar is fixed on one of the bearing shafts, whereas the other side can slide as well as rotate through a cylindrical joint. Therefore, the left and right arms of the parallel mechanism are not exactly symmetric. In this study, we assume the two shoulder motors are fixed, and the two elbow motors are utilized to generate the motion of lion head in six directions (three rotations and three translations). The motors at shoulders and torso can be used to compensate motion range of the end-effector such as the nodding and turning motion of lion head.

B. Number of Degree-of-freedom

The number of degree-of-freedom of this 2-DOF parallel manipulator can be calculated from following equation:

$$M = 6(n - g - 1) + \sum_{i=1}^{g} f_i, \tag{1}$$

where M is the number of DOFs of the mechanism, n is the number of bodies in the mechanism, g is the number of joints and f_i is the number of DOFs of the i^{th} joint. For this parallel arm structure, $n = 7$ (as illustrated in Fig. 1(a)), $g = 7$, $f_i = 1$ for each of the revolute joints, and $f_i = 2$ for the cylindrical joint. Application of Eqn. (1) yields

$$M = 6(7 - 7 - 1) + 6 \times 1 + 2 = 2. \tag{2}$$

It can be seen that the number of DOFs is consistent with that of motors. Therefore, the system is neither over constraint nor under constraint.

III. Forward Kinematic Analysis

Forward kinematics is the process of relating a system's pose to the position and orientation of the end effector. It is widely used in robotics, computer games, and animation. In this study, the end effector (such as lion head) is mounted on the horizontal bar on top of the arm structure. The purpose of kinematic analysis is to describe the position as well as orientation of the lion head by using the rotation angles of the two elbow motors. There are six parameter to completely define the end-effector in 3D space, i.e., three displacement parameters utilized for determining the position of point O' on the end-effector and three angular parameters for the orientation of the end-effector. To facilitate the following discussion, we assume that the bar goes through the two revolute joints at B_1 and B_2.

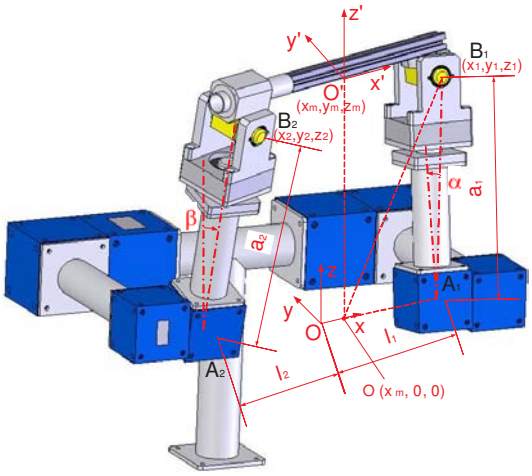

Fig. 2. Coordinates definition on the arm structure

A. Formulation of Forward Kinematics

As illustrated in Fig. 2, two Cartesian coordinate systems are employed for the forward kinematic analysis, i.e., global coordinates (x, y, z) that is fixed on the base of the system, and local coordinates (x', y', z') that is fixed on the bar or the end-effector. According to the geometric relationship presented in Fig. 2, the following equations can be found

$$\begin{aligned} x_1 &= l_1, \\ y_1 &= a_1 \sin\alpha, \\ z_1 &= a_1 \cos\alpha, \end{aligned} \tag{3}$$

and

$$\begin{aligned} x_2 &= -l_2, \\ y_2 &= -a_2 \sin\beta, \\ z_2 &= a_2 \cos\beta, \end{aligned} \tag{4}$$

where (x_1, y_1, z_1), (x_2, y_2, z_2) are defined on the global coordinate system (x, y, z). Note that the directions of α and β

are opposite. Because the three points (x_1, y_1, z_1), (x_2, y_2, z_2) and (x_m, y_m, z_m) are on a line (ignore the offset of the bar), it can be obtained that

$$\frac{x_m - x_1}{x_2 - x_1} = \frac{y_m - y_1}{y_2 - y_1} = \frac{z_m - z_1}{z_2 - z_1} = t, \tag{5}$$

$$(x_m - x_1)^2 + (y_m - y_1)^2 + (z_m - z_1)^2 = l_1^2, \tag{6}$$

which results in,

$$[(x_2 - x_1)^2 + (y_2 - y_1)^2 + (z_2 - z_1)^2]t^2 = l_1^2. \tag{7}$$

Therefore,

$$t = l_1 / \sqrt{[(x_2 - x_1)^2 + (y_2 - y_1)^2 + (z_2 - z_1)^2]}. \tag{8}$$

The coordinates of (x_m, y_m, z_m) can be expressed in terms of $x_1, y_1, z_1, x_2, y_2, z_2$ as

$$x_m = x_1 + (x_2 - x_1) l_1 / \sqrt{[(x_2 - x_1)^2 + (y_2 - y_1)^2 + (z_2 - z_1)^2]}, \tag{9}$$

$$y_m = y_1 + (y_2 - y_1) l_1 / \sqrt{[(x_2 - x_1)^2 + (y_2 - y_1)^2 + (z_2 - z_1)^2]}, \tag{10}$$

$$z_m = z_1 + (z_2 - z_1) l_1 / \sqrt{[(x_2 - x_1)^2 + (y_2 - y_1)^2 + (z_2 - z_1)^2]}. \tag{11}$$

By using Eqns. (9) - (11) and Eqns. (3) - (5), the position of O' can be computed from the motors' position α and β. The next step is to formulate the orientation of the bar from α and β. First, the direction of x' in the global frame can be calculated as

$$\begin{aligned} \overrightarrow{x'} &= [x_1 - x_2, y_1 - y_2, z_1 - z_2]^T \\ &= \begin{bmatrix} l_1 + l_2 \\ a_1 \sin\alpha + a_2 \sin\beta \\ a_1 \cos\alpha - a_2 \cos\beta \end{bmatrix}. \end{aligned} \tag{12}$$

Similarly,

$$\begin{aligned} \overrightarrow{A_1 B_1} &= [x_1 - l_1, y_1, z_1]^T \\ &= \begin{bmatrix} 0 \\ a_1 \sin\alpha \\ a_1 \cos\alpha \end{bmatrix}. \end{aligned} \tag{13}$$

The vector of y' is the cross product of $\overrightarrow{x'}$ and $\overrightarrow{A_1 B_1}$

$$\begin{aligned} \overrightarrow{y'} &= \overrightarrow{A_1 B_1} \times \overrightarrow{x'} \\ &= \begin{bmatrix} a_1 s\alpha(a_1 c\alpha - a_2 c\beta) - a_1 c\alpha(a_1 s\alpha + a_2 s\beta) \\ a_1 c\alpha(l_1 + l_2) \\ -a_1 s\alpha(l_1 + l_2) \end{bmatrix}, \end{aligned} \tag{14}$$

where $s\beta$, $c\beta$, $s\alpha$, $c\alpha$ represent $\sin\beta$, $\cos\beta$, $\sin\alpha$ and $\cos\alpha$ respectively. The direction of z' is

$$\overrightarrow{z'} = \overrightarrow{x'} \times \overrightarrow{y'} = \begin{bmatrix} (-a_1 + a_2 s\alpha c\beta - a_2 s\alpha s\beta) a_1 (l_1 + l_2) \\ -a_1 a_2 (a_1 c\alpha - a_2 c\beta)(s\alpha c\beta + c\alpha s\beta) + (l_1 + l_2)^2 a_1 s\alpha \\ a_1 \{(l_1 + l_2)^2 c\alpha - (a_1 s\alpha + a_2 s\beta)[s\alpha(a_1 c\alpha - a_2 c\beta) - c\beta(a_1 s\alpha + a_2 s\beta)]\} \end{bmatrix}. \tag{15}$$

Thus, the orientation of the lion head with respect to the global coordinates can be represented with following matrix

$$\mathbf{R}_1 = \begin{bmatrix} \frac{\overrightarrow{x'}}{\|\overrightarrow{x'}\|} & \frac{\overrightarrow{y'}}{\|\overrightarrow{y'}\|} & \frac{\overrightarrow{z'}}{\|\overrightarrow{z'}\|} \end{bmatrix} = \begin{bmatrix} r_{11} & r_{12} & r_{13} \\ r_{21} & r_{22} & r_{23} \\ r_{31} & r_{32} & r_{33} \end{bmatrix}. \tag{16}$$

On the other hand, the rotational matrix can be represented with Euler angles. Suppose that the lion head starts with the frame coincident with the global frame, then rotates about z' axis by an angle of θ_z, and then rotates about y' axis by angle of θ_y, finally rotates about x' axis by an angle of θ_x. The general rotation matrix after these three rotations can be represented as [14]

$$\mathbf{R}_2 = \begin{bmatrix} c\theta_z c\theta_y & c\theta_z s\theta_y s\theta_x - s\theta_z c\theta_x & c\theta_z s\theta_y c\theta_x + s\theta_z s\theta_x \\ s\theta_z c\theta_y & s\theta_z s\theta_y s\theta_x + c\theta_z c\theta_x & s\theta_z s\theta_y c\theta_x - c\theta_z s\theta_x \\ -s\theta_y & c\theta_y s\theta_x & c\theta_y c\theta_x \end{bmatrix}. \tag{17}$$

where $s\theta_x$, $c\theta_x$, $s\theta_y$, $c\theta_y$, $s\theta_z$, $c\theta_z$ represent $\sin\theta_x$, $\cos\theta_x$, $\sin\theta_y$, $\cos\theta_y$, $\sin\theta_z$ and $\cos\theta_z$ respectively. Comparing the elements in $\mathbf{R}_1$ and $\mathbf{R}_2$ gives

$$\begin{aligned} \theta_y &= \arctan[-r_{31} / (\sqrt{r_{11}^2 + r_{21}^2})], \\ \theta_z &= \arctan[r_{21} / \cos\theta_y / (r_{11} / \cos\theta_y)], \\ \theta_x &= \arctan[r_{32} / \cos\theta_y / (r_{33} / \cos\theta_y)]. \end{aligned} \tag{18}$$

B. Simulation of Forward Kinematics

1) Variation of Displacement Parameters: Let $a_1 = a_2 = 400$mm and $l_1 = l_2 = 150$mm. By using Eqns. (9)-(11), the variations of x_m, y_m and z_m with respect to the motor angles α and β are plotted as shown in Fig. 3. In Fig. 3(a), it can be seen that x_m is always equal to zero when $\alpha = -\beta$. This result can be observed in Fig. 3(d), i.e., O' is on the plane of xOy ($x_m = 0$) when two arms move in the same direction and the same magnitude. However, from Fig. 3(a), when $\alpha \neq -\beta$, $x_m > 0$. This is because the bar is fixed at the point B_1, and thus the distance between the end-effector (O') and B_1

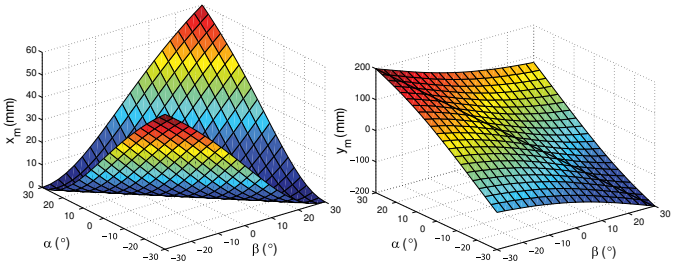

(a) Variation of x_m (b) Variation of y_m

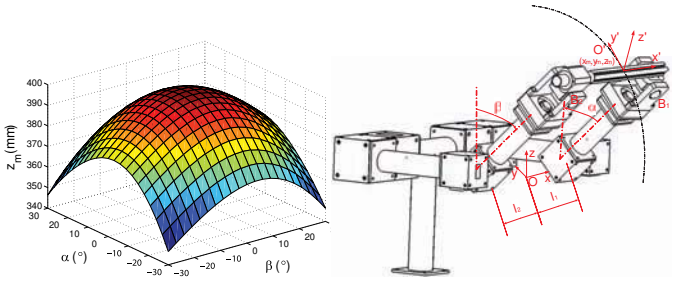

(c) Variation of z_m (d) Robotic arms

Fig. 3. Displacement of point O' with respect to motor angles α and β

is fixed. When $\alpha \neq -\beta$, O' is dragged to the left arm side, i.e. $x_m > 0$. Figure 3(b) shows the variation of y_m. When $\alpha = -\beta$, y_m varies from positive value (when $\alpha > 0$) to negative value (when $\alpha < 0$). This variation can be observed in Fig. 3(d). Similarly, from Fig. 3(c), it can be clearly seen that z_m reaches the highest value when the two arms are at the upright position whereas z_m becomes smaller when motors are in any other positions, which is consistent with the inspection from Fig. 3(d).

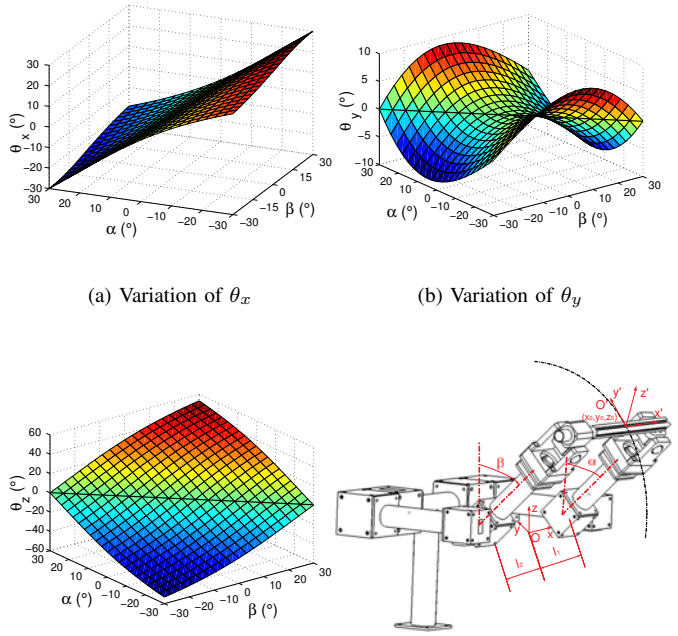

(a) Variation of θ_x (b) Variation of θ_y

(c) Variation of θ_z (d) Robotic arms

Fig. 4. Angular displacement of point O' with respect to α and β

2) Variation of Angular Parameters: The angular motions of end-effector with respect to local coordinates x', y' and z' are presented in Fig. 4. According to Fig. 4(d), when $\alpha = -\beta$, i.e., the two arms move in the same direction as well as same speed, there is only rotational motions about x' axis, whereas the angular displacement about y' and z' are equal to zero. This fact coincides with the data variation plotted in Fig. 4(b) and 4(c) (the black line across the plotting surface).

IV. Inverse Kinematic Analysis

Inverse kinematics is the process of determining the parameters of a jointed flexible object (a kinematic chain) in order to achieve a desired pose. In this study, the purpose of inverse kinematic analysis is to derive motor angles α and β from the orientation of the end-effector. Because this is a 2-DOF mechanism, θ_z and θ_x are selected as two independent parameters to represent the nodding and shaking motion of the end-effector (lion head).

A. Formulation of Inverse Kinematics

By comparing r_{11} in $\mathbf{R}_1$ with the corresponding element in $\mathbf{R}_2$, following equation can be obtained

$$\tan\theta_z = \frac{a_1\sin\alpha + a_2\sin\beta}{l_1 + l_2}. \tag{19}$$

Similarly, comparing r_{31} and r_{32} with corresponding elements in $\mathbf{R}_2$ gives

$$\frac{\sqrt{(l_1+l_2)^2 + (a_1\sin\alpha + a_2\sin\beta)^2}\,\sin\theta_x}{\sqrt{(l_1+l_2)^2 + a_1^2 + a_2^2 + 2a_1a_2(\sin\alpha\sin\beta - \cos\alpha\cos\beta)}} = \frac{-a_1\sin\alpha(l_1+l_2)}{\sqrt{[a_1^2a_2^2(\sin\alpha\cos\beta + \cos\alpha\sin\beta)]^2 + a_1^2(l_1+l_2)^2}}. \tag{20}$$

From Eqns. (19) and (20), the two unknowns, α and β can be solved numerically.

B. Simulation Result of Inverse Kinematics

The simulation result of α and β with respect to θ_x and θ_z is presented in Fig. 5. From Fig. 4(d), it can be seen that when $\theta_z = 0$ and $\theta_x \neq 0$, the two motor angles move in the same direction, i.e., $\alpha = -\beta$. This result can be observed in Fig. 5. With reference to the black bold line in Fig. 5, the value of α decreases with the increase of θ_x ($\theta_z = 0$). However, the variation of β with respect to θ_x ($\theta_z = 0$) is opposite to that of α, yet in the same magnitude.

V. Workspace Analysis

The purpose of this section is to analyze the workspace of the humanoid arm structure by using the kinematic analysis result. Workspace is the volume of space which the end-effector of the manipulator can reach. There are two types of workspace, dextrous workspace and reachable workspace. Dextrous workspace is the volume of space which the robot end-effector can reach with all orientations. The reachable workspace is the volume of space which the end-effector can reach in at least one orientation. Clearly, the dextrous workspace is a subset of reachable workspace. It can be found that there is no dextrous workspace for this proposed humanoid arm structure because the end-effector cannot achieve all orientations at any point in the workspace. Therefore, the workspace study here focuses on the reachable workspace.

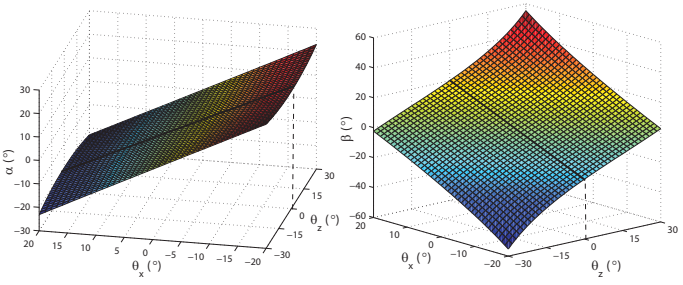

(a) Variation of α (b) Variation of β

Fig. 5. Variation of α and β

A. Workspace Computation and Visualization

By using Eqns. (9)-(11), the workspace of the arm structure is computed numerically and presented in Fig. 6. To facilitate the understanding, the explaination of the workspace is broken down into four steps as follows.

Step one: Figure 6(a) represents the position of end-effector (point O') when $\alpha = -\pi/4$ and β varies from $-\pi$ to π. It can be seen that the trajectory of end-effector is a closed 3D curve in the space.

Step two: Let $\alpha = \pi/4$ and β varies from $-\pi$ to π. Another 3D curve that is symmetric to the previous one with respect to the plane of $y_m = 0$ is obtained as shown in Fig. 6(b).

Step three: Subsequently, let α vary from $-\pi/4$ to $\pi/4$, and β vary from $-\pi$ to π. It can be found from Fig. 6(c) that a set of 3D curves similar to the one in Fig. 6(a) form a shell of cylindrical surface. It is noted that the shape of all those curves are the same.

Step four: Finally, varying both α and β from $-\pi$ to π gives the workspace of the arm structure as shown in Fig. 6(d). From the figure, it can be found that the value of x_m is always greater than zero, which is due to the fact that the distance from point O' to B_1 is fixed (l_1). When the two motors move, point O' will be dragged to a position where x_m is greater than zero. Apparently, the workspace of the arm structure is the shell of a cone-shaped solid. Every cross section of the workspace parallel to the plane of $x_m = 0$ is a circle centering at (0, 0, 0). In other words, for a given x_m, $y_m^2 + z_m^2$ is always equal to a certain fixed positive value. This phenomenon is verified in following section.

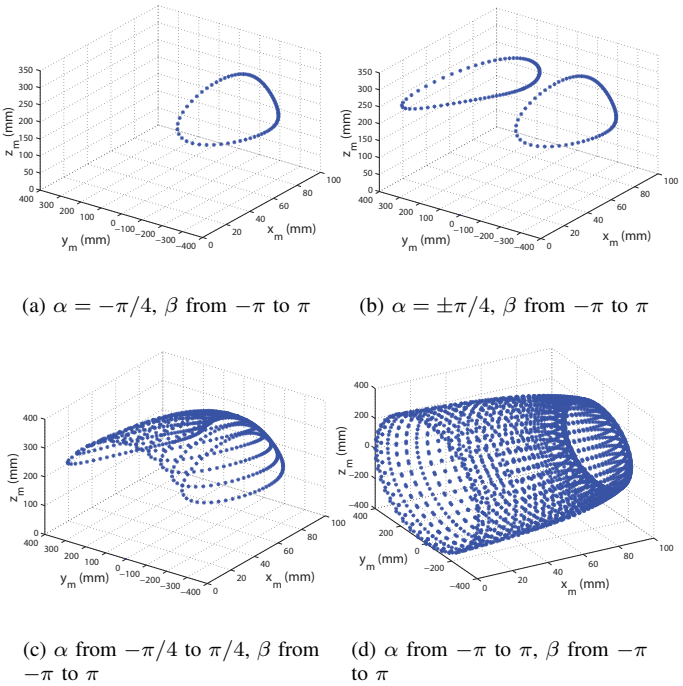

(a) $\alpha = -\pi/4$, β from $-\pi$ to π

(b) $\alpha = \pm\pi/4$, β from $-\pi$ to π

(c) α from $-\pi/4$ to $\pi/4$, β from $-\pi$ to π

(d) α from $-\pi$ to π, β from $-\pi$ to π

Fig. 6. Workspace of the arm structure

B. Verification of $y_m^2 + z_m^2 > 0$

To prove that $y_m^2 + z_m^2$ is a fixed positive value, in the first place, it is necessary to prove that it is not equal to zero, i.e., y_m and z_m cannot both be zero. To prove the impossibility of this situation, let $y_m = 0$ and $z_m = 0$, and see what would happen. Obviously, with $y_m = 0$ and $z_m = 0$, Eqn. (6) becomes

$$(x_1 - x_m)^2 + y_1^2 + z_1^2 = l_1^2. \tag{21}$$

In terms of geometry, Eqn. (21) means that the distance between a point (x_m, 0, 0) and the other one (x_1, y_1, z_1) is equal to l_1. With reference to Fig. 2, points O'', B_1 and O' form a triangle. Because $\angle B_1O'O'' \geq \pi/2$, it is always greater than $\angle O'O''B_1$. Thus, $\|B_1O''\| > \|O'B_1\|$, i.e.

$$(x_1 - x_m)^2 + y_1^2 + z_1^2 > l_1^2, \tag{22}$$

which is contradict with Eqn. (21). Therefore, the assumption of $y_m = 0$ and $z_m = 0$ is not correct, i.e., $y_m^2 + z_m^2$ is greater than zero.

The next step is to prove that $y_m^2 + z_m^2$ is a fixed value for a given x_m. According to Eqn. (9), a constant value of x_m indicates that the value of $x_1 + (x_2 - x_1)l_1/\sqrt{[(x_2 - x_1)^2 + (y_2 - y_1)^2 + (z_2 - z_1)^2]}$ is constant. Furthermore, because x_1 and x_2 are constants, $\sqrt{[(x_2 - x_1)^2 + (y_2 - y_1)^2 + (z_2 - z_1)^2]}$ (denoted as C_{x_1,y_1,z_1}) is a constant too. Substituting Eqns. (3) and (4) into C_{x_1,y_1,z_1} shows that

$$C_{\alpha,\beta} = \sin\alpha\sin\beta - \cos\alpha\cos\beta \tag{23}$$

is a constant value. From Eqns. (3), (4) and (9)-(11), the following result can be achieved

$$y_m^2+z_m^2=a_1^2-\frac{2a_1a_2C_{\alpha,\beta}+2a_1^2}{C_{x_1,y_1,z_1}}l_1+\frac{a_1^2+a_2^2+2a_1a_2C_{\alpha,\beta}}{C_{x_1,y_1,z_1}^2}l_1^2. \tag{24}$$

From Eqn. (24), it can be seen that the right side of the equation is a constant. Thus, by combining the result of Step one, the value of $y_m^2 + z_m^2$ is always a fixed positive value for a given x_m. In other words, a cross section of the workspace of the arm structure parallel to the plane of $x_m = 0$ (Fig. 6(d)) is a circle centering at (0, 0, 0).

VI. Prototype and Implementation

A prototype of the humanoid arm structure has been developed as shown in Fig. 7. Two Powercube motors are employed to drive the elbows, and two are used to drive shoulders. The two elbow motors can generate the end-effector motion in six translational and rotational directions. The two shoulder motors and two torso motors (only show one torso motor in the figure) can compensate the motion range of the arm structure.

This humanoid arm structure is successfully implemented to a lion dancing system for holding the lion head. As shown in Fig. 8(a), lion dance is a form of traditional dance in Chinese culture, in which performers mimic a lion's movements in a lion costume. The lion costume may be operated by a single dancer, or more frequently by a pair of dancers who form the

Fig. 7. Prototype of the arm structure

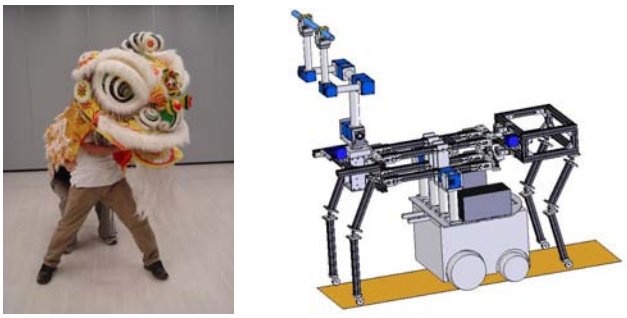

(a) Human dancing (b) Robotic lion

Fig. 8. Robotic lion dancing system

back and fore legs of the lion. In recent years, biomimetic (Biomimetic refers to human-made processes, substances, devices, or systems that imitate nature.) robotics develops very fast because it exhibits much greater robustness in performance in unstructured environments than today's robots. In our research, we proposed a robotic lion dancing system that uses advance robotic technology to develop a mechatronic system (Fig. 8(b)) that can perform life-size lion dancing with the traditional lion dance outfit, and thus the traditional art form and robotic technology can be fused to stimulate people's interest in disappearing traditional art form as well as give new meanings to the new art form. One of the major components in the robotic lion system is the humanoid arm structure, on which the lion head will be mounted to move in six directions. Because only two motors are used to drive the arms' motion to achieve the end-effector motion, the power consumption of the robotic lion is reduced greatly. By using this structure, the lion head can achieve a vivid motion in three translational directions and three rotational directions.

VII. Conclusion

A 2-DOF parallel mechanism is proposed for the design of humanoid arm structure in this paper. The asymmetric architecture is employed to achieve the end-effector motion in six directions. Only two motors are used to reduce the system power consumption as well as the total cost. Based on the concept design, the forward kinematics and inverse kinematics are analyzed and visualize. Furthermore, the 3D workspace of the end-effector is computed and presented. A prototype of the humanoid arm structure is developed and successfully implemented into the robotic lion dancing system, which shows that the humanoid arm structure can generate a lively motion of the lion head in six directions.

Acknowledgment

This work is a collaborative research project between Nanyang Technological University and Singapore Institute of Manufacturing Technology. The authors acknowledge the assistance from Ms. Ang Gim Ching Jenny, Mr. Han Boon Siew and Mr. Ho Wee Kiat Desmond.

References

[1] V. E. Gough and S. G. Whitehall, "Universal tyre test machine," in *Proceedings of the 9th FISITA, International Automobile Technical Congress*, 1962, pp. 117–137.

[2] D. Stewart, "A platform with six degrees of freedom," in *Proceedings of Institution of Mechanical Engineers*, vol. 180 (15), 1965, pp. 371–386.

[3] J. P. Merlet, "Workspace-oriented methodology for designing a parallel manipulator," in *Proceedings of the 1996 IEEE International Conference on Robotics and Automation*, Minnesota, USA, 1996, pp. 3726–3731.

[4] Q. Li and Z. Huang, "Type synthesis of 5-dof parallel manipulators," in *Proceedings of the 2003 IEEE International Conference on Robotics and Automation*, Taipei, Taiwan, September 2003, pp. 14–19.

[5] X. Kong and C. M. Gosselin, "Type synthesis of 5-dof parallel manipulators based on screw theory," *Journal of Robotic Systems*, vol. 22, no. 10, pp. 535–547, 2005.

[6] J. Angeles, A. Morozov, and O. Navarro, "A novel manipulator architecture for the production of scara motions," in *In Proceedings of the 2000 IEEE International Conference on Robotics and Automation*, San Francisco, CA, USA, April 2000, pp. 2370–2375.

[7] P.-L. Richard, C. M. Gosselin, and X. Kong, "Kinematic analysis and prototyping of a partially decoupled 4-dof 3t1r parallel manipulator," *Journal of Mechanical Design*, vol. 129, pp. 611–616, 2007.

[8] X. Kong and C. M. Gosselin, "Type synthesis of 3t1r 4-dof parallel manipulators based on screw theory," *IEEE Transactions on Robotics and Automation*, vol. 20, no. 2, pp. 181–190, 2004.

[9] R. Clavel and S. A. Sogeva, "Device for the movement and positioning of an element in space," *US Patent*, no. 4,976,582, December 1990.

[10] C. Gosselin and J. Angeles, "The optimum kinematic design of a spherical three-degree-of-freedom parallel manipulator," *ASME Journal of Mechanisms, Transmission, and Automation in Design*, vol. 111, pp. 202–207, 1989.

[11] K.-M. Lee and D. Shah, "Kinematics analysis of a three-degree-of-freedom in-parallel actuated manipulator," *IEEE Journal of Robotics and Automation*, vol. 4, no. 3, pp. 354–360, 1988.

[12] M. A. N. J. A. Carretero, R. P. Podhorodeski and C. M. Gosselin, "Kinematic analysis and optimization of a new three degree-of-freedom spatial parallel manipulator," *ASME Journal of Mechanical Design*, vol. 122, pp. 17–24, 2000.

[13] J. A. Carretero, M. A. Nahon, and R. P. Podhorodeski, "Workspace analysis of a 3-dof parallel mechanism," in *Proceedings of the 1998 IEEE/RSJ International Conference on Intelligent Robots and Systems*, Victoria, B.C., Canada, 1998, pp. 1021–1026.

[14] J. J. Craig, *Introduction to Robotics: Mechanics and Control*. USA: Addison-Wesley Publishing Company, 1989.